Case Studies in Thermal Engineering 51 (2023) 103575

Contents lists available at ScienceDirect

Case Studies in Thermal Engineering

journal homepage: www.elsevier.com/locate/csite

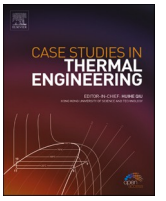

Experimental investigations of particle sizes effects on exergy and entropy characteristics of AL_2O_3 - MWCNT hybrid nanofluid along the transitional flow regime

Ibrahim Umar Ibrahim [a,b], Mohsen Sharifpur [a,c,*], Josua P. Meyer [a,d]

[a] Department of Mechanical and Aeronautical Engineering, University of Pretoria, Pretoria, 0002, South Africa
[b] Department of Mechanical Engineering, Ahmadu Bello University Zaria, Kaduna State, Nigeria
[c] Medical Research Department, China Medical University Hospital, China Medical University, Taichung, Taiwan
[d] Department of Mechanical and Mechatronic Engineering, Stellenbosch University, Stellenbosch, South Africa

ARTICLE INFO

Keywords:
Thermal entropy
Frictional entropy
Hybrid nanofluids
Transitional regime
Heat transfer

ABSTRACT

Experimental investigation on particle size effect on entropy and exergy characteristics of AL_2O_3 - MWCNT hybrid nanofluid in transitional flow Regime was carried out with four different particle sizes (i.e., for Aluminum oxide (AL_2O_3), 20 nm, and 5 nm used while Multiwalled Carbon Nanotubes (MWCNT) <7 nm and 30–50 nm particles). 0.3 vol concentrations of three hybrid nanofluids with different particle size combinations (i.e., Al_2O_3(20 nm) – MWCNT(20–30 nm), Al_2O_3(20 nm) – MWCNT(<7 nm), and then Al_2O_3(5 nm) – MWCNT(<7 nm)) are prepared using a two-step method, at a percentage weight composition (PWC) of 60:40. Results shows that Nanofluid with Al_2O_3 (20 nm) and MWCNT (<7 nm) have shown the best performance. It has an exergy efficiency of 54.12% at turbulent Reynold number of 4500, while in the transitional flow regime, it records an exergy efficiency of 47.85%. Frictional entropy and thermal entropy in the transitional regime were reduced with hybrid nanofluid of Al_2O_3 (20 nm) and MWCNT (<7 nm) by 6.78% and 13.53%, respectively, as compared to Al_2O_3 (5)- MWCNT (<7) nanofluid. Both thermal and frictional entropy effects were better minimized in the turbulent regime than in the lamina and transitional regime, as they were reduced by 16.66 and 24.7%, respectively. The study also recommends that for further investigations, more samples need to be taken to reach a clearer conclusion the effect of particle size, and since this is a hybrid nanofluid the samples should be of different sizes from both nanoparticles.

Nomenclature

$Ex_{dest,T}$	Thermal Exergy Destruction
k_{cu}	Thermal conductivity of the copper
$Ex_{dest,f}$	Frictional Exergy Destruction
h_{avg}	Average Coefficient of Heat transfer
φ	Volume concentration
k	Thermal Conductivity

* Corresponding author. Department of Mechanical and Aeronautical Engineering, University of Pretoria, Pretoria, 0002, South Africa.
E-mail address: mohsen.sharifpur@up.ac.za (M. Sharifpur).

https://doi.org/10.1016/j.csite.2023.103575
Received 15 May 2023; Received in revised form 27 September 2023; Accepted 30 September 2023
Available online 1 October 2023

A_s	Surface Area
c_p	Specific heat capacity of Particles
c_{hnf}	Specific heat capacity of Hybrid Nanofluid
Re	Reynold Number
Pr	Prandtl
P	Perimeter of the tube
$T_{so}(x)$	Outside wall temperature
D_{so}	Outer Tube Diameter
$\dot{m}$	Mass flow Rate
$T_f(x)$	Local Mean Fluid Temperature
D_{si}	Internal Tube diameter
T_i	Inlet Temperature
$\dot{Q}_f$	Heat Transfer Rate
$h(x)$	Heat transfer coefficient
$\dot{q}_{in}$	Heat flux
$S_{g,f}$	Frictional Entropy
η_{ex}	Exergy Efficiency
EB	Energy Balance
$\dot{Q}_e$	Electric Energy Supply Rate
x	Distance from the tube inlet
ρ_{hnf}	Density of the Hybrid nanofluids
ρ_p	Density of Particles
ρ_{bf}	Base fluid density
T_a	Ambient Temperature
$S_{g,total}$	Total Entropy
c_{bf}	Specific heat capacity of base
V	Voltage
L	Test Section Length
D_o	Outer Diameter
D_i	Internal Diameter
$T_{si}(x)$	Inside wall temperature
Nu_{avg}	Average Nusselt Number
Be	Bejan Number
I	Current
$S_{g,T}$	Thermal Entropy

Greek Letters

μ	viscosity
ν	Kinematic viscosity
ρ	Density

Subscripts

o	Outlet/Out
i	Inlet
f	fluid
s	Surface
a	Ambient/Atmospheric
avg	Average

Abbreviations

PWC	Percentage weight compositions
NDE	Non- Dimensional Exergy Destruction
IDR	Irreversibility distribution ration

1. Introduction

Nanofluid Heat transfer characteristics and capabilities are still under investigation. So much still needs to be discovered or not fully understood about these enhanced working fluids that show promising signs of improving thermal management. Especially in this

current age where technological advancement is on the rise, thermal management is one of the serious issues that put a limit on the capabilities of these new advanced systems [1,2]. One important thing that needs consideration is entropy generation because the estimation of entropy generation provides information about the irreversibility that occurs within the system. Tharayil et al. [3] explained that entropy generation is used in thermodynamics to analyze the performance of various thermal systems, whereby the system with the lowest entropy is thought to perform better. It is not new that nanofluid's properties vary due to different factors, including volume concentration, types and sizes of particles, method of preparation, etc. Maheshkumar et al. [4] explained that entropy is affected by several factors that are independent of the fluid properties, like heat pipe dimensions. Therefore, entropy generation could be significantly minimized by adequately selecting pipe dimensions, Khalkhali et al. [5] found that optimum ambient temperature and dimensions are crucial to minimizing entropy generation, similar findings were also reported by Bhattad et al. [6] where a decrease in application temperature results in a reduction of exegetics performance.

With regards to nanofluid performance evaluation using entropy analysis, more research is still needed to investigate their entropy generation, especially in tube flow. Singh et al. [7] investigate the nanofluids entropy generation using different tube diameter results show that tubes with big diameter sizes experience higher Thermal entropy than smaller tubes. At the same time, frictional entropy appears to be much higher in small-size tubes, this was consistent with results presented by Ziapour et al. [8]. Ghanbarpour et al. [9] investigated the performance of Aluminum oxide (Al_2O_3) and Titanium oxide (TiO_2) water nanofluid, research findings indicate that nanofluid performance is better than that of the base fluid (i.e., water) as the total entropy generation was reduced to about 3–13% with nanofluids of 1–5% volume concentration and their performance increase with nanoparticle loading in the base fluid, Al_2O_3 - water nanofluid has minimized entropy generation more than TiO_3 and the base fluid. Jafarmadar et al. [10] investigate water-based nanofluid of Al_2O_3, CuO, and silver performance on entropy generation, where silver (Ag) entropy generations appear to be much higher when compared to the other fluid tested. Tharayil et al. [3] also reported a reduction in entropy generations using a 0.6% volume concentration of graphene-water nanofluid. Zhao et al. [11] report a significant entropy generation degradation with TiO_2. While Sundar et al. [12] prepared a nanodiamond + Fe_3O_4 hybrid fluid with water-ethylene as base fluid and reported a 20% reduction in thermal entropy generation. Sardarabadi et al. [13] applied metal oxide nanofluid on the photovoltaic thermal system (PVT), and an enhancement of 15.93% in exergy efficiency was reported. Bhattad et al. [14] also reported an improvement in exergy efficiency of 0.5% with aluminium-cupper hybrid nanofluid. Findings of the experimental works of Safarzadeh et al. [15], Sundar et al. [16], and Bhattad et al. [17]revealed that fluid entropy generation is affected by an increase in particle concentration.

Another important factor that was investigated and found to have significant effects on the nanofluid's entropy characteristics is the Particle shapes. Alanazi et al. [18] used Aluminum oxide nanoparticles of different shapes, which include blade, cylinder, and platelet-shaped particles. Results show that at a volume concentration of 1% platelet-shaped particles, nanofluid have reduced the entropy generation and frictional effect in the system more than the blade and cylindrical-shaped particles. Rafique et al. [19] also reported that the shapes of the particles significantly impact both fluid's heat transfer and entropy generation because findings from the numerical simulation show that Os-shaped particles were far better than the rest of the particle Shapes investigated in the research. Similarly, Alqaed et al. [20] reported that Os shaped to perform better. This reaffirmed the findings of Rafique et al. [19]. Also, Bhattad et al. [21] investigated the effects of both particle shapes and sizes on the thermohydraulic performance of plate evaporator, their findings reaffirmed that particle shapes have a strong significance on the heat transfer and their performance index, while heat transfer area was found to be reduced with increase in particles size. In a similar research, Bhattad et al. [22] investigated the effects of inlet temperature on the thermodynamic characteristic of Hybrid nanofluid of Aluminium-graphene and Aluminium – water nanofluid, in this research, it was found out that with the of nanofluid, second low efficiency deteriorates while irreversibility rate and non-dimensional exergy (NDE) increases.

Research on the effects of particle sizes on heat transfer characteristics are very few, especially with the hybrid nanofluid, even though research has shown that particle sizes have a significant influence on tube convective heat transfer characteristic, Anoop et al. [23] and Bhattad et al. [21]. Very few works use hybrid nanofluids. Our findings have shown that no work yet investigates the influence or impacts of particle sizes on the hybrid nanofluid entropy generation therefore, in this current work, we investigate the effects or influence of particle sizes on hybrid nanofluids' entropy generation. It was already established that the use of nanofluid has an impact on reducing the entropy generation compared to base fluid [9–16]. This current work aims not to compare nanofluid performance with base fluid but rather to investigate and analyze the influence of particle sizes on entropy only. Al_2O_3 – MWCNT was chosen because of the research work of Ghanbarpour et al. [9], Bhattad et al. [14], and Jafarmadar et al. [10] all reported a significant entropy minimization with the Al_2O_3 nanofluid, and also due to its good stability, as reported by Osman et al. [22], while MWCNT has a very high thermal conductivity. In an interesting work also, Bhattad et al. [24] analysed the economic importance ofhybrid nanofluids, results show that Aluminium base hybrid nanofluids have appreciably low annual costs. However, the main goal of the present work is to study the thermal behaviour of hybrid nanofluids as a case study for the impact of particle sizes. Three hybrid nanofluids of Al_2O_3 – MWCNT are prepared at a 0.3% volume concentration, the particle sizes used are 5 nm and 20 nm for Al_2O_3 and <7 nm, and 30–50 for Multiwalled carbon Nanotubes are used.

2. Experimentation

2.1. Preparations Al_2O_3 – MWCNT Nanofluid

Deionized water (DI – Water) was used as the base fluid to prepare the three hybrid nanofluids of Al_2O_3 and MWCNT nanoparticles. Using the two-step method, four different particle sizes were used (i.e., Al_2O_3 (20 nm), MWCNT (<7 nm), Al_2O_3 (5 nm), and MWCNT (30–50 nm). These particles were hybridized using a 60:40 ratio (60% by weight percentage of Aluminium and 40% by weight percentage of MWCNT). 60:40 hybridization ratio was chosen because Krishnan et al. [25], experiments on the properties of hybrid

nanofluid (Al_2O_3 - MWCNT/DI-water) at various particle weight ratios explained that 60:40 exhibits the best thermal properties. 0.3 vol concentration was prepared and used in this experimental study, 0.3 concentration was chosen because Hameed et al. [26] reported that, its performance is by far the best compared to 0.2 and 0.1 vol concentrations. The nanofluid combinations prepared are Al_2O_3 (5 nm)-MWCNT (<7 nm), Al_2O_3 (20 nm)-MWCNT (<7 nm), and Al_2O_3 (20 nm)-MWCNT (30–50 nm). Fig. 1(a–c) shows the SEM images of the three hybrid nanoparticles as supplied by the Manufacturers (US Research Nanomaterial (USA)) with average particle sizes of 20 nm and 5 nm for Al_2O_3 and 7 and 30–50 for Multi-Walled Carbon Nanotube. Magnetic stirring (30min) and sonication at an amplitude of 90 for 1 h were used, breaking down the agglomerates generated and dispersing them (i.e., nanoparticles) in the base fluid.

2.2. Stability and thermophysical properties of the hybrid nanofluid

Nanofluids stability ware examined by measuring and monitoring the viscosity at a constant temperature of 20 °C, the viscosity readings were taken using Sv–10 Vibro Viscometer (A&D, Japan), which is set to record and login data at an interval of 10 min for 4.5 h, as shown in Fig. 2. In all cases of experiments, the system got steady in about 90 min, therefore, the nanofluids in the experimental set-up were stable during the experimentations. A similar method was also used by Osman et al. [27] and Giwa et al. [28,29]. Fluids were also visualized and monitored for ten days without any sedimentation, which shows that they have good stability, and this agreed with Krishnan et al. [30]. They prepared and tested the same hybrid nanofluid's properties and stability using similar methods and parameters.

Fig. 3a illustrates the hybrid nanofluids' thermal conductivity as measured by a KD2 Pro thermal conductivity meter at various temperatures ranging from 20 °C to 60 °C. Results were compared with the thermal conductivity correlation of Pack and Cho [31] presented in Equation (1), and the correlation differs by less than 3% from the measured outcome. This is similar to the findings of Sharma et al. [32].

$$k_{nf} = k_w(1 + 7.47\varphi) \tag{1}$$

Fig. 3b presents the viscosity of the hybrid nanofluid between the temperatures of 20 °C–60 °C

The viscosity is compared to the viscosity of water and with the regression Equation (2), as Presented in Fig. 3b. The comparison was similar to the method used by Sharma et al. [32] and Osman et al. [27]. And the regression equation (2) correlates very well with nanofluid data.

$$\mu_{nf} = \mu_w\left(1 + 2.5\varphi + 6.2\varphi^2\right) \tag{2}$$

Fig. 4 presents the pH and electrical conductivity data for the hybrid nanofluids. Al_2O_3 (5) – MWCNT (<7) has the highest pH, whereas Al_2O_3 (20) – MWCNT (30–50) has the lowest pH, nanofluids pH appeared to decrease with increasing temperature, which is consistent with the findings of Giwa et al. [33] and Krishnan et al. [30].

The result of the electrical conductivity of the hybrid nanofluid is also presented in (Fig. 4b),

electrical conductivity increases as the temperature increases, which is similar to the finding of Giwa et al. [33].

The density of the hybrid nanoparticles was computed using equation (3), which Sundar et al. [34] recommended and applied, and it was discovered to be 3.222 kg/m^3. Equation (4) was used to determine the hybrid nanoparticles' specific heat.

$$\rho_{(Al_2O_3-MWCNT)} = \frac{\left(\rho_{Al_2O_3} PWC_{Al_2O_3}\right) + \left(\rho_{MWCNT} PWC_{MWCNT}\right)}{\left(PWC_{Al_2O_3} + PWC_{MWCNT}\right)} \tag{3}$$

$$c_{(Al2O3-MWCNT)} = \frac{\left(c_{Al_2O_3} PWC_{Al_2O_3}\right) + \left(c_{MWCNT} PWC_{MWCNT}\right)}{PWR_{Al_2O_3} + PWR_{MWCNT}} \tag{4}$$

PWC is the Percentage weight concentration of the nanoparticles in the Hybrid nanofluids, where Aluminium is 60, and MWCNT is 40, and deionized water is utilized as the base fluid and has a 999kg/m3 density.

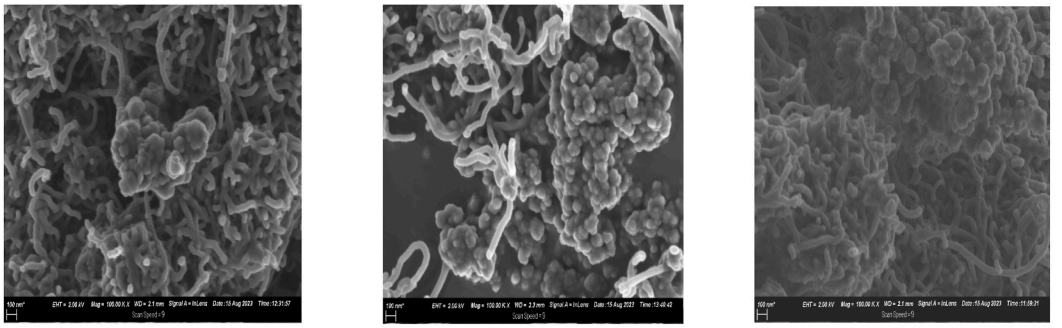

a) Al_2O_3 (20 nm) and MWCNT (< 7 nm) b) Al_2O_3 (5 nm) and MWCNT (< 7 nm) c) Al_2O_3 (20 nm) and MWCNT (30-50nm)

Fig. 1. SEM images of the hybrid nanoparticles.

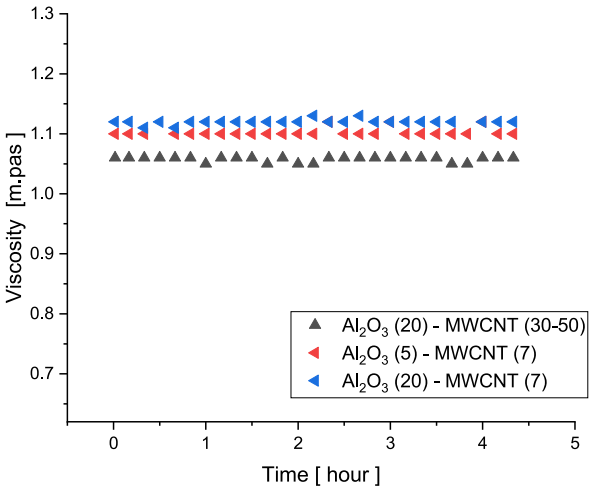

Fig. 2. Stability checking at 20 °C for 4hr 30min.

Hybrid nanofluid density and heat capacity were obtained from the relations developed from the research work of Pak and Cho [35], and used by Sundar et al. [36] and Naik et al. [28], as shown here in equations (5) and (6):

$$\rho_{\mathrm{hnf}} = (1-\varphi)\rho_{\mathrm{bf}} + \varphi\rho_p \tag{5}$$

$$C_{\mathrm{hnf}} = (1-\varphi)C_{\mathrm{bf}} + \varphi C_p \tag{6}$$

Where, ρ_{hnf} , c_{hnf}, φ , ρ_{bf} , c_{bf}, c_p are nanofluid density, heat capacity (specific), concentration, the density of the water (deionized water), the heat capacity (specific) of the DI water, the heat capacity (specific) of the hybrid nanoparticles, and density of the hybrid nanoparticles, respectively.

2.3. Experimental set-up

The fundamental design of the set-up is presented in Fig. 5. Force convection test equipment consists of a tank (for fluid storage) (8) capable of storing and supplying 10 L of water/Nanofluid for use during testing using a gear pump (1). The power was supplied to the test section to provide a continuous heat flux to the heat exchanger section, which heats the fluid from an inlet temperature (T_{in}) to an output temperature (T_{out}). To minimize heat loss, the heated test section was thoroughly insulated with insulation materials with a thickness of about 70 mm (comprising 6 layers of tight insulation). The fluid exited the heated test section through a flow meter. The flow meter has 0.05% accuracy when operating at full capacity (4), and a heat exchanger (5) cooled the hot fluid (from Test sections (3)) where the heat was dumped into cold water from a Thermal bath (6), and the temperature at the test section's inlet was kept constant. The system was equipped with a data collection system that receives and analyses signals from the power supply, flow meters, thermocouples, and pressure transducers in a computer (9). The data was logged in using a Lab View application that was designed to log data at a frequency of 20 Hz.

2.4. Experimental procedure

The system had to be allowed to stabilize for at least 1.5 h after starting up to achieve a steady state. When there are no apparent variations in temperature, flow rate, and pressure values, a steady state is thought to have been reached. After the system stabilized, minor modifications were made to the flow rates to obtain a new flow rate for data capture. It takes roughly 10 min for the system to return to its steady state after changing the flow rate (higher to a lower flow). Data was captured from the higher flow rate to the lower flow rate to minimize leftover heat from being stored in the insulation and influencing subsequent readings; for each data point analysis, 200 readings were recorded by the data acquisition systems and averaged for data analysis.

3. Data analysis and validation

The method of Data analysis method used for this research work is similar to the method followed by Meyer et al. [37].
The fluid heat transfer $h(x)$ coefficient obtained from the relation,

$$h(x) = \frac{\dot{q_{in}}}{T_{si}(x) - T_f(x)} \tag{7}$$

where $\dot{q_{in}}$ is the heat flux, computed from the rate of energy supplied $\dot{Q_e}$

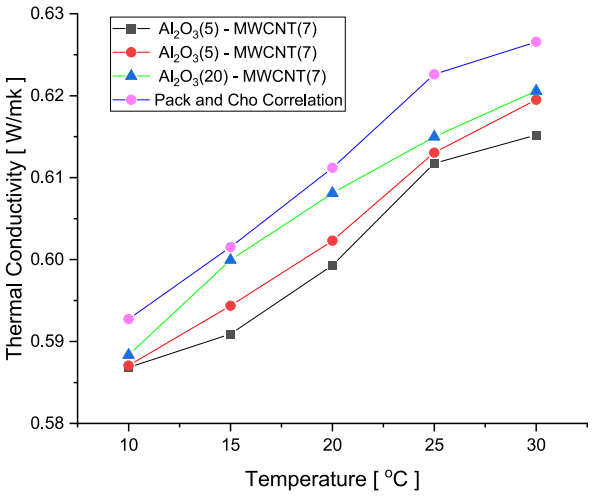

a) Thermal conductivity

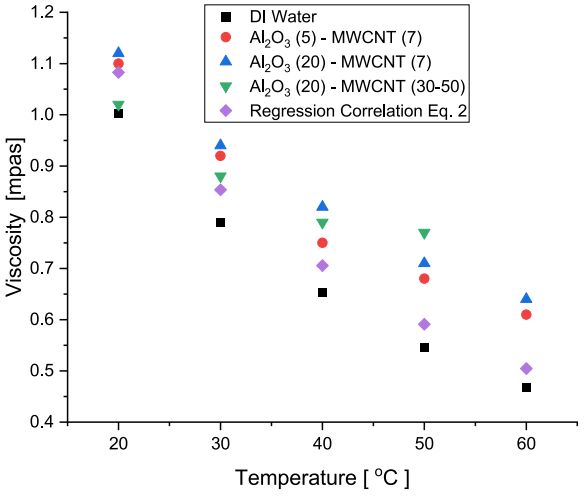

b) Viscosity of hybrid nanofluids

Fig. 3. **a)** Thermal conductivity and **b)** Viscosity of hybrid nanofluids.

$$\dot{Q}_e = VI \tag{8}$$

Then heat flux, $\dot{q}_{in}$ is calculated as given in equation (9).

$$\dot{q}_{in} = \frac{\dot{Q}_e}{A_S} \tag{9}$$

A_s is the Tube's internal Surface Area.

$$A_s = \pi DL \tag{10}$$

The heat transfer rate $\dot{Q}_f$ to the fluid was determined from the mass flow rate, inlet and outlet temperature, and Specific heat capacity measured at a bulk temperature.

$$\dot{Q}_f = \dot{m} c_p (T_{out} - T_{in}) \tag{11}$$

The heat transfer rate $\dot{Q}_f$ which is monitored throughout the experiments to ensure constant heat flux is supplied and is compared

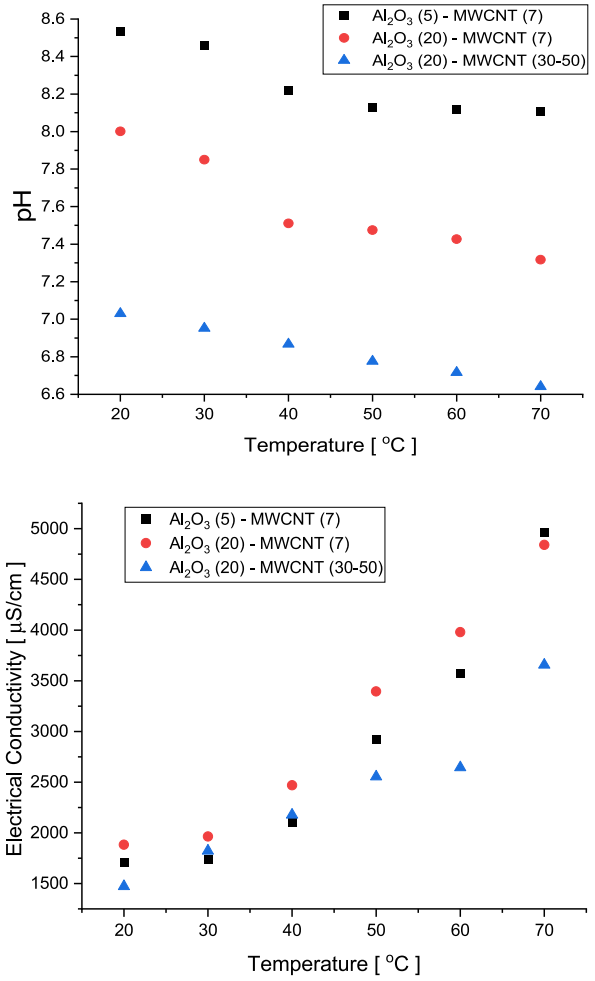

Fig. 4. **a)** pH value and **b)** Electrical conductivity of hybrid nanofluids.

to electrical energy supplied. The energy balance (EB) is computed as follows.

$$EB = \left| \frac{\dot{Q}_e - \dot{Q}_f}{\dot{Q}_e} \right| \times 100 \tag{12}$$

The energy balance of all the experiments was less than 3%, showing that the tube is well insulated.

Throughout the experiment, a constant heat flux of 8.67 kW/m^2 is provided to the system.

The local inner surface temperatures $T_{si}(x)$ and $T_f(x)$ were calculated using outer wall temperature, $T_{so}(x)$ and resistance through the tube wall, (R_w) as shown below.

$$\mathrm{T_{si}(x) T_{so}(x) - q_{in} R_w} \tag{13}$$

Were.

$$R_w = \frac{\ln \frac{D_{so}}{D_{si}}}{2\pi k_{cu} L} \tag{14}$$

k_{cu} is the tube material(copper) Thermal conductivity and is computed as defined by Ref. [38] and applied by Meyer et al. [29], While local mean fluid Temperature T_f was obtained from the relation.

$$T_f(x) = T_i + \frac{\dot{q}_{in} x p}{\dot{m} c_p} \tag{15}$$

Where p is the Perimeter of the tube.

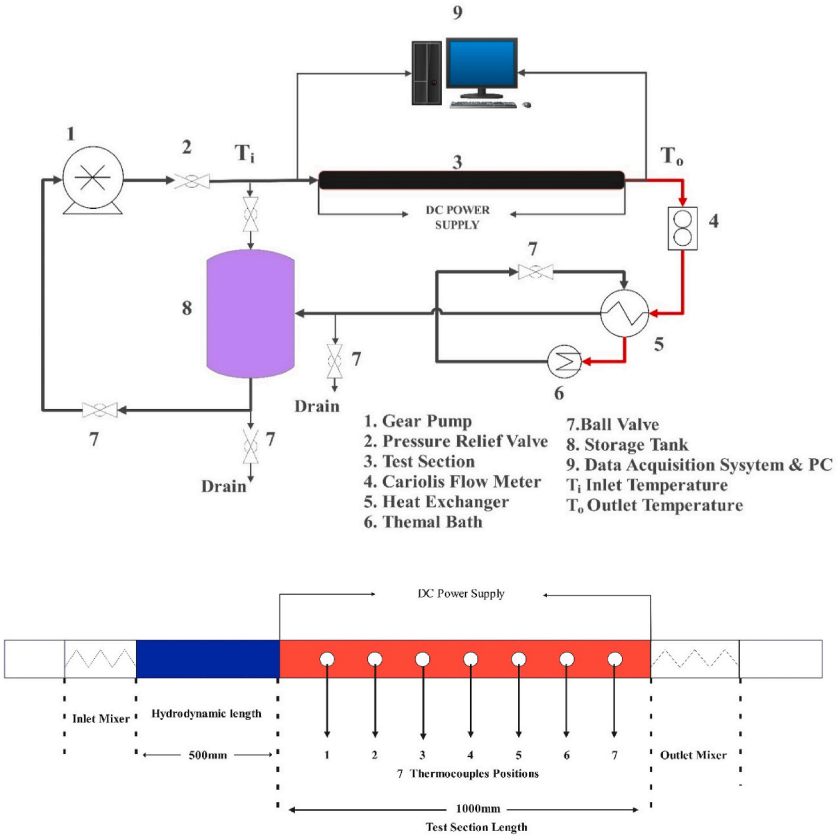

Fig. 5. Schematic diagram of test setup and the test section.

The coefficient of convective heat transfer (Average), h_{avg} was determined by averaging the preceding equation (7) along the tube length at all seven thermocouple points, Thus, by averaging the convective coefficient of heat transfer $h(x)$ (local) at all thermocouple locations.

$$h_{avg} = \frac{(h(x_1) + h(x_2) + h(x_3) + \ldots\ldots h(x_n))}{n} \tag{16}$$

Where, n = 7.

The working fluid's (i.e., hybrid nanofluid) Prandtl and Reynold Numbers were computed using the following relations.

Reynold Number *Re*

$$Re = \frac{4m}{\pi DL} \tag{17}$$

Prandtl Number *Pr*.

$$\mathrm{P}r = \frac{\mu c_p}{k} \tag{18}$$

Average Nusselt's number was obtained from h_{avg} in equation (16).

$$Nu_{avg} = \frac{h_{avg} D}{k} \tag{19}$$

k represent the Thermal conductivity, of water, it was determined using the correlation developed by Popiel et al. [39] at fluid bulk temperature T_b.

$$f = \frac{\nabla_p}{\left(\frac{L}{d_i}\right)\left(\frac{\rho v^2}{2}\right)} \tag{20}$$

3.1. Entropy analysis

Entropy Analysis of the hybrid nanofluid is done using equations (21)–(23) [16,40,41].

$$\dot{S}_{g,Total} = \dot{S}_{g,T} + \dot{S}_{g,f} \tag{21}$$

$$\dot{S}_{g,T} = \frac{\dot{Q}_f^{\,2}}{Nu\pi k T_{out} T_{in} L} \tag{22}$$

The Nusselt's Number (*Nu*) is computed by using equation (19).

$$S_{g,F} = \frac{8fm^3 L}{\rho^2 \pi^2 D_i^{\,5} (T_{out} - T_{in})} \ln\left(\frac{T_{out}}{T_{in}}\right) \tag{23}$$

Where, $S_{gtotal} S_{g,T}$ and $S_{g,f}$ represent the total Entropy, thermal (Heat) Entropy, and frictional entropy generation, respectively, $\dot{Q}_f$ while represents the heat transfer rate [16].

Bejan number, Exergy efficiency, Thermal Exergy Destruction, and Frictional Exergy Destruction, are expressed in equations (24-27). Sundar et al. [16].

$$Be = \frac{S_{g,T}}{S_{g,T} + S_{g,F}} \tag{24}$$

3.2. Exergy analysis

$$\eta_{ex} = 1 - \frac{T_a S_{g,T}}{\left[1 - \left(\frac{T_a}{T_s}\right)\right] \times \dot{Q}_f} \tag{25}$$

Thermal Exergy Destruction

$$Ex_{dest,T} = T_a S_{g,T} \tag{26}$$

Frictional Exergy Destruction

$$Ex_{dest,f} = T_a S_{g,f} \tag{27}$$

Non – Dimensional Exergy Destruction (NDE)

NDE is computed from the relation given in equation (28) As given by Bhattad et al. [14].

$$NDE = \frac{1}{\dot{m} c_p (T_{out} - T_{in})} \tag{28}$$

3.3. Validation of the setup

The experimental results were compared to correlations from Dittus – Boelter [42], Gnielinski [43], and Notter-Rouse [44]. To

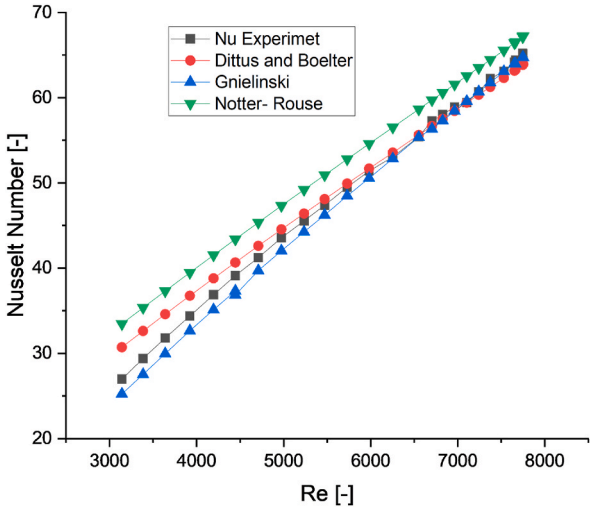

Fig. 6. Validation of the Experimental Setup using Correlation.

which the experimental data strongly correlate with these connections. as illustrated in Fig. 6. The correlation of Dittus - Boelter, Gnielinski, and Notter-Rouse compares with experimental data in the turbulent domain. However, when compared to the other correlations, the Gnielinski correlation predicts the outcome quite well. It underpredicts the outcome by less than 3% on average. This enhances confidence in the Data capturing and Analysis method and justifies the research procedure, design, and data reduction strategy.

4. Result and discussion

Theoretically, the transition regime starts at an approximate Critical Reynold number of 2300 Cengal et al. [45], but research works by Meyer and Oliver [46], Nagendra et al. [47], and Ghajar and Tam [48] explained that the start of the transition is affected by several factors, which includes inlet configuration, heat flux, fluid properties, etc. also Osman et al. [27] found out that transition starts early with nanofluid than with the base fluid, (water) and this due to the increase in the fluid viscosity. In this research, the start and end of the transition regime are identified using the method suggested by Everts et al. [49] and Andrade et al. [50] in which they defined the critical Reynold number (Re_{cr}) as the Reynold number at which the Colburn j factor gradient is equal to zero, as given by Equation (29)

$$\mathrm{Re} = \mathrm{Re}_{cr}, \text{When } \mathrm{Re} = \left(\frac{dj}{d\mathrm{Re}}\right) = 0 \tag{29}$$

The range of the transition (Start and End) for the three hybrid nanofluids is found to be between the Reynold number of 1150 and 2700. Data are taken between the Reynold number of 400–5000, which covers lamina and turbulent regimes.

4.1. Entropy generation

4.1.1. Thermal entropy generation

From the experimental results presented in Fig. 7a, thermal entropy generation along the lamina and transitional region appeared to have a higher value than in the turbulent regions. It was noticed that the thermal entropy value reduces with an increase in the Reynold number, and this is consistent with the finding of Sundar et al. [12], which investigated the nanofluid entropy generation along the turbulent regime, similar results were also reported by Mehrali et al. [51] and for both the three fluids Al_2O_3 (5)- MWCNT (<7) have the highest thermal entropy in the transitional region. While minimizing thermal entropy is key to enhancing the exergetic performance of a system because higher thermal entropy signifies higher system irreversibility [16]. Results show that at a turbulent Reynold number of 4500 (Re ≈ 4500), there is thermal entropy degradation with Al_2O_3 (20)- MWCNT (<7) of about 24.7% compared to the Al_2O_3 (5)- MWCNT (<7), while along the transitional flow, Al_2O_3 (20)- MWCNT (<7) there is a reduction in thermal entropy of about 13.53% when compared to the Al_2O_3 (5)- MWCNT (<7) nanofluid.

4.1.2. Frictional entropy generation

Presented in Fig. 7b, entropy generation due to frictional effect (Frictional entropy), is unlike entropy due to heat transfer (i.e., Thermal entropy), it increases as the Reynold number increases, similar findings were also reported in the works of Sundar et al. [12], Mehrali et al. [51] and [16] results show that there is a reduction in frictional entropy with Al_2O_3 (20)- MWCNT (<7) nanofluid as compared with the other two fluids (Al_2O_3 (20)- MWCNT (30–50), and Al_2O_3 (5)- MWCNT (<7)). At a turbulent Reynold number of 4500 (Re ≈ 4500), and a Transitional Reynold number of 2000 (Re = 2000) there is a reduction in frictional entropy generation of about 16.66% and 6.78% as compared to the Al_2O_3 (5)- MWCNT (<7) nanofluid.

4.2. Exergy destruction

4.2.1. Thermal exergy destruction

Nanofluids' thermal exergy destructions are presented in Fig. 8a, like thermal entropy, thermal exergy destructions also decrease with the increase in Reynold number, which is Similar to the results reported by [12,16,41]. Hybrid nanofluid with Particle sizes of Al_2O_3 (20 nm) and MWCNT (<7 nm) particles have the lowest thermal exergy destructions when compared with the other two fluids investigated, there is a reduction in thermal exergy destruction with Al_2O_3 (20)- MWCNT (<7) nanofluid of about 47.0% at Turbulent Reynold number of 4500 while at transition Region (Re = 2000) the reduction is for about 6.22% when compared with the Al_2O_3 (5)- MWCNT (7) nanofluid this makes it very obvious, that particles sizes influence the thermal characteristics of these fluids, as it was

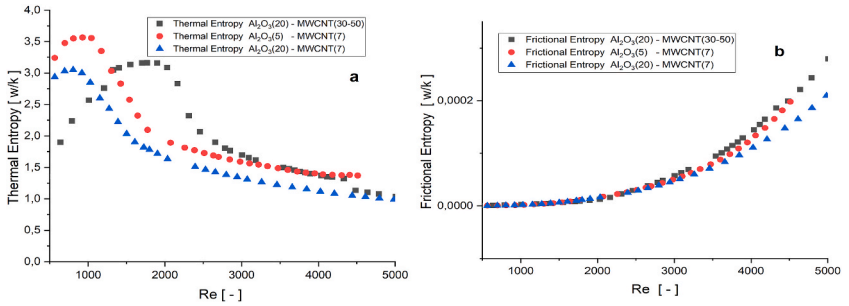

Fig. 7. (a) Thermal (heat) entropy generation against the Reynold number; (b) frictional entropy generation against the Reynold number.

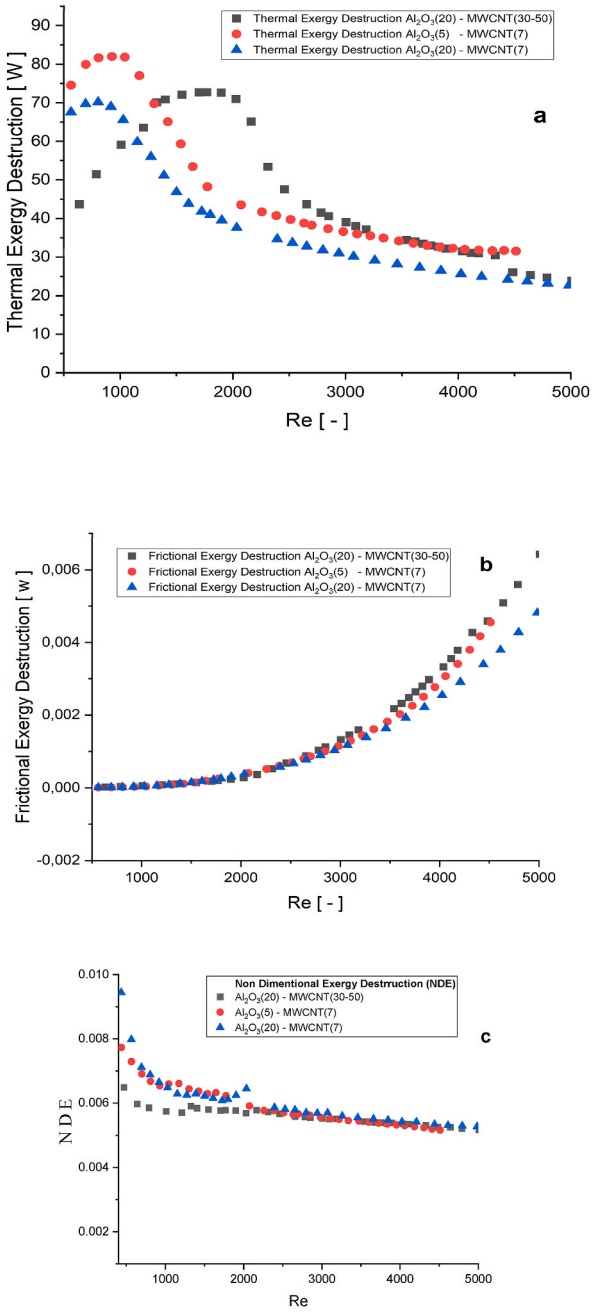

Fig. 8. (a) Frictional Exergy Destruction against Reynold Number; (b) Thermal Exergy Destruction against Reynold Number c) Non-Dimensional Exergy Destruction against Reynold Number.

confirmed with other parameters like volume concentration.

4.2.2. *Frictional exergy destruction*

Fig. 8b shows the frictional exergy destruction graph, for the three hybrid nanofluids of Al_2O_3 – MWCNT, nanofluids with particles combination of Al_2O_3 (20 nm) and MWCNT (<7 nm), have the lowest frictional exergy destruction among all the fluid tested, it has a reduction of about 16.68% in the turbulent region as compared to the Al_2O_3 (5)- MWCNT (<7), while in the Transitional region, it has recorded a reduction of about 6.78% compared to the Al_2O_3 (5)- MWCNT (<7).

4.2.3. *Non-dimensional exergy destruction*

Hybrid nanofluid Non-dimensional Exergy Destruction (NDE) is presented in Fig. 8c. Results show that NDE decreases with an increase in Reynold. For both the three hybrid nanofluid fluids, its magnitude is very much higher at the lamina regime than in

transitional and turbulent, this was consistent with the findings reported by Bhattad et al. [16], where NDE reduces with an increase in flow rate. Al_2O_3 (20 nm) - MWCNT (30–50) have the lowest NDE in the lamina region, compared to the rest fluids. However only a slight difference was noticed in the turbulent and transitional regions.

4.3. Bejan Number

As presented in Fig. 9, and equation 24 Bejan is described as the ratio of Thermal entropy to the sum total of entropy generation in the system, (i.e., the sum total of the entropies as a result of friction (frictional) and Thermal entropy). Bejan number is very significant with regard to fluid thermal analysis, it helps to access the effects and influence of the frictional exergy destructions and pressure drop in the system. When the Bejan number approaches one, it signifies the reductions in the impact of frictional exergy destruction on the system, which also means that there is low irreversibly in the system, a higher Bejan number signifies that entropy generation due to fluid heat transfer is higher than frictional entropy of the system [12], which also reflects that the system irreversibility distribution ratio (IDR) is high, because IDR is the relative measure of heat transfer influence on the irreversibility, as explained by Bhattad et al. [17] Bejan number helps to visualize the effect of heat transfer on the pressure drop. Bejan value also decreases with the increase in the Reynold number, because of the increase in the frictional exergy destructions of the system. Fig. 8b shows that the frictional exergy destruction of the system is increasing with the rise in the Reynold number, that's the reason the Bejan value reduces with the rise in the Reynolds number. At a low Reynold number, its value is nearly equal to 1, (i.e., lamina region). Still, as the Reynold number increases, it keeps reducing gradually, it's important to note that the Bejan Number can't be 1, because we cannot eliminate all the irreversibility in the system. Fig. 9 shows the results of the Bejan number plotted against the Reynolds number, this result was similar to the findings of [12], [16], [51]. Reduction in the Bejan number also shows an augmentation in the pressure drop and fluid pumping power, which are all associated with the frictional entropy of the system. Due to the effects of different particle sizes, their Bejan number value was also affected for the fluid tested here. Fig. 9 shows that hybrid nanofluid fluid Al_2O_3 (20 nm) and MWCNT(20–30) have the highest Bejan number reduction in the turbulent region of flow compared to the Nanofluid with the particle combinations of Al_2O_3 (20 nm) - MWCNT(<7 nm) which indicates that the rise in fluid pumping power and frictional effects with Al_2O_3 (20 nm) -MWCNT(20–30), is higher than that of the Al_2O_3 (20 nm) and MWCNT(<7 nm)

4.4. Exergy efficiency

Fig. 10 present the exergy efficiency plot of the three hybrid nanofluids Al_2O_3 - MWCNT with water as base fluid, these three fluid differ with each other only by the Particles sizes combination of the Aluminium and MWCNT, but from the result of the exergy efficiency, it's shows that their performance as a heat transfer fluid differs significantly, which confirmed that nanoparticles sizes have significant effects on the thermal and heat transfer performances of nanofluids, Nanofluids of the Al_2O_3 (20 nm) and MWCNT(<7 nm), appeared to have the highest exergy efficiency among the fluids tested, at turbulent Reynolds number of 4500, Al_2O_3 (20 nm) and MWCNT(<7 nm) nanofluid have an exergy efficiency of about 54.12%, whereas the Al_2O_3 (20 nm) – MWCNT(30–50 nm), recorded only 29.82% exergy efficiency, while along the transitional flow regime (Re 2000) nanofluid with particles sizes combination of Aluminium 20 nm and Multiwalled carbon nanotubes <7 nm, have an exergy efficiency of 47.85% while fluid with the particle sizes Al_2O_3 (20 nm) – MWCNT(30–50 nm), have 6.16% exergy efficiency, this was due to the effect of the of frictional exergy destruction, and fluid pumping power, as we have seen in the frictional entropy, frictional exergy destructions results. It shows that nanofluids with 20 nm and <7 nm particle sizes have less frictional exergy destruction than other fluids. Therefore, it can be said that hybrid nanofluid particle size combinations have a critical role in influencing the thermal characteristics of these fluids, there is a need to carefully analyze and choose the optimum particle sizes for better fluid performances, of Nanofluid as a heat transfer fluid.

5. Conclusion

Three hybrid nanofluids of Al_2O_3 and MWCNT are prepared using a two-step method of Nanofluid preparation, that is, by dispersing particles in Deionized water, at a mixing ratio of 60:40%, 0.5 wt% of SDBS was added as a surfactant, these three fluid have different particles size combinations, prepared at the same volume concentrations of 0.3, to investigate the effects of particles sizes on nanofluid exergy and entropy generation, the particles sizes used are; Al_2O_3 (20 nm and 5 nm) and MWCNT (<7 nm and 30–50 nm), from the experimental results, the following observations were made;

From the experimental results analysed, it was observed that nanofluid particle sizes have significant effects on thermal characteristics; results revealed that fluid frictional entropy, Thermal entropy generation, and exergy destructions were all affected by varying the particle sizes of the same fluids at the same volume concentration. It became more evident with the fluid exergy efficiency, where nanofluid with particle combination of Al_2O_3 (20 nm) and multiwalled (<7 nm), shows the highest exergy efficiency of about 54.12%, in the turbulent regime. In contrast, along the transitional region, it has an exergy efficiency of 47.85%, which is remarkable when compared to the Al_2O_3 (20 nm) – MWCNT (30–50 nm), which recorded only 29.82% exergy efficiency, in the turbulent flow and 6.16% in the transition regime.

It's also noted that exergy efficiency in the transition flow regime is more affected by the effects of particle sizes than the turbulent region, because the differences in fluid performance in the region are very high, which is because frictional exergy and friction exergy destructions are more significant in the region. As mentioned earlier, at a transitional Reynold number of Re ≈ 2000, Al_2O_3 (20 nm) – MWCNT (30–50 nm), only managed to record an exergy efficiency of 6.16%, while at the same Reynold number Al_2O_3 (20 nm) – MWCNT(<7 nm) has an exergy efficiency of 47.85%. A conclusion was attained that, hybrid nanofluid heat transfer performances can be improved by properly selecting the particle sizes, especially for the heat exchanger designed to operate along the transition regime.

The study also recommends that for further investigations, more samples need to be taken to reach a clearer conclusion the effect of

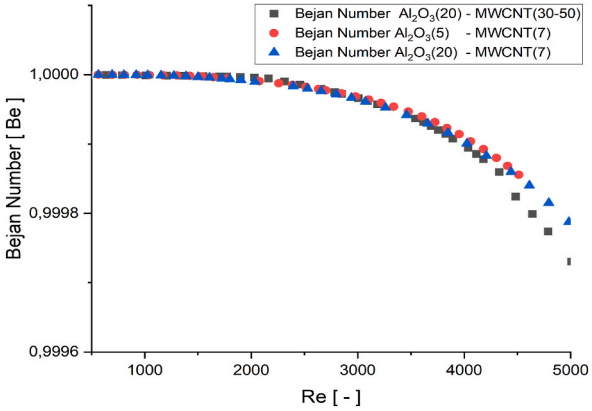

Fig. 9. Bejan number against the Reynold number.

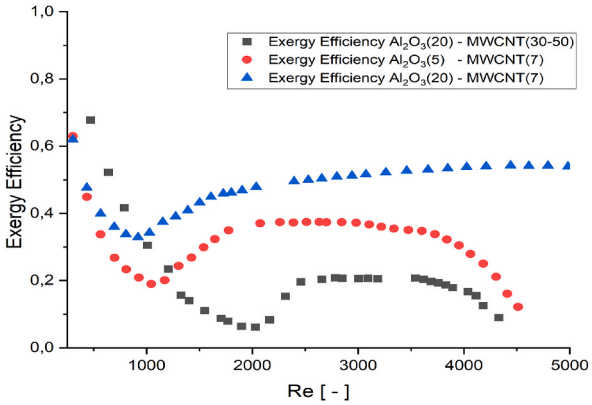

Fig. 10. Graph of exergy efficiency against the Reynold number.

particle size, and since this is a hybrid nanofluid the samples should be of different sizes from both nanoparticles.

CRediT author statement

Ibrahim Umar Ibrahim: Data acquisition, Methodology, Experimental work, Validation, Results Interpretation, Writing the original draft, Mohsen Sharifpur: Methodology, Validation, Writing and editing, Supervision, Funds., Josua P. Meyer: Methodology, Reviewing and Editing, Co-supervision.

Declaration of competing interest

The authors declare that they have no known competing financial interests or personal relationships that could have appeared to influence the work reported in this paper.

Data availability

Data will be made available on request.

References

[1] Bhattad, et al., Review on mono and hybrid nanofluids: preparation, properties, investigation, and applications in IC engines and heat transfer, Energies 16 (2023) 3189, https://doi.org/10.3390/EN16073189, vol. 16, no. 7, p. 3189, Mar. 2023.
[2] I.U. Ibrahim, M. Sharifpur, O. Manca, J.P. Meyer, Nanofluid's Convective Heat Transfer for Laminar, Transitional, and Turbulent Flow," Nanofluid Applications for Advanced Thermal Solutions, Jan. 2023, pp. 151–192, https://doi.org/10.1016/B978-0-443-15239-9.00006-0.
[3] T. Tharayil, L.G. Asirvatham, M.J. Dau, S. Wongwises, Entropy generation analysis of a miniature loop heat pipe with graphene–water nanofluid: thermodynamics model and experimental study, Int. J. Heat Mass Tran. 106 (2017), https://doi.org/10.1016/j.ijheatmasstransfer.2016.08.035.
[4] P. Maheshkumar, C. Muraleedharan, Minimization of entropy generation in a flat heat pipe, Int. J. Heat Mass Tran. 54 (2011), https://doi.org/10.1016/j.ijheatmasstransfer.2010.09.006, 1–3.
[5] H. Khalkhali, A. Faghri, Z.J. Zuo, Entropy generation in a heat pipe system, Appl. Therm. Eng. 19 (10) (1999), https://doi.org/10.1016/S1359-4311(98)00089-1.

[6] A. Bhattad, J. Sarkar, P. Ghosh, Exergetic analysis of plate evaporator using hybrid nanofluids as secondary refrigerant for low-temperature applications, Int. J. Exergy 24 (1) (2017) 1–20, https://doi.org/10.1504/IJEX.2017.086857.

[7] P.K. Singh, K.B. Anoop, T. Sundararajan, S.K. Das, Entropy generation due to flow and heat transfer in nanofluids, Int. J. Heat Mass Tran. 53 (2010), https://doi.org/10.1016/j.ijheatmasstransfer.2010.06.016, 21–22.

[8] B.M. Ziapour, H. Shaker, Exergetic analysis of a long two-phase closed thermosyphon system, Int. J. Exergy 7 (6) (2010), https://doi.org/10.1504/IJEX.2010.035517.

[9] M. Ghanbarpour, R. Khodabandeh, Entropy generation analysis of cylindrical heat pipe using nanofluid, Thermochim. Acta 610 (2015), https://doi.org/10.1016/j.tca.2015.04.028.

[10] S. Jafarmadar, N. Azizinia, N. Razmara, F. Mobadersani, Thermal analysis and entropy generation of pulsating heat pipes using nanofluids, Appl. Therm. Eng. 103 (2016), https://doi.org/10.1016/j.applthermaleng.2016.03.032.

[11] N. Zhao, C. Qi, T. Chen, J. Tang, X. Cui, Experimental study on influences of cylindrical grooves on thermal efficiency, exergy efficiency and entropy generation of CPU cooled by nanofluids, Int. J. Heat Mass Tran. 135 (2019), https://doi.org/10.1016/j.ijheatmasstransfer.2019.01.106.

[12] S. Sundar, S. Mesfin, E. Venkata Ramana, Z. Said, A.C.M. Sousa, Experimental investigation of thermo-physical properties, heat transfer, pumping power, entropy generation, and exergy efficiency of nanodiamond + Fe3O4/60:40% water-ethylene glycol hybrid nanofluid flow in a tube, Therm. Sci. Eng. Prog. 21 (2021), https://doi.org/10.1016/j.tsep.2020.100799.

[13] M. Sardarabadi, M. Hosseinzadeh, A. Kazemian, M. Passandideh-Fard, Experimental investigation of the effects of using metal-oxides/water nanofluids on a photovoltaic thermal system (PVT) from energy and exergy viewpoints, Energy 138 (2017), https://doi.org/10.1016/j.energy.2017.07.046.

[14] A. Bhattad, Exergic performance of plate evaporator coated with nanoparticles for fish preservation. https://doi.org/10.1080/14484846.2023.2217966, 2023, 10.1080/14484846.2023.2217966.

[15] S. Safarzadeh, M. Niknam-Azodi, A. Aldaghi, A. Taheri, M. Passandideh-Fard, M. Mohammadi, Energy and entropy generation analyses of a nanofluid-based helically coiled pipe under a constant magnetic field using smooth and micro-fin pipes: experimental study and prediction via ANFIS model, Int. Commun. Heat Mass Tran. 126 (2021), https://doi.org/10.1016/j.icheatmasstransfer.2021.105405.

[16] L. Syam Sundar, Experimental study on the thermophysical properties, heat transfer, thermal entropy generation and exergy efficiency of turbulent flow of ZrO2-water nanofluids, Alex. Eng. J. 65 (2023), https://doi.org/10.1016/j.aej.2022.10.001.

[17] A. Bhattad, J. Sarkar, and P. Ghosh, "Energetic and exergetic performances of plate heat exchanger using brine-based hybrid nanofluid for milk chilling application,"Heat Trans. Eng. https://doi.org/10.1080/01457632.2018.1546770, vol. 41, no. 6–7, pp. 522–535, Apr. 2019, Doi: 10.1080/01457632.2018.1546770..

[18] K. Alanazi, Y. Khetib, H.M. Abo-Dief, M. Rawa, G. Cheraghian, M. Sharifpur, The effect of nanoparticle shape on alumina/EG-water (50:50) nanofluids flow within a solar collector: entropy and exergy investigation, Case Stud. Therm. Eng. 28 (Dec. 2021), 101510, https://doi.org/10.1016/J.CSITE.2021.101510.

[19] K. Rafique, Z. Mahmood, S. Saleem, S.M. Eldin, U. Khan, Impact of nanoparticle shape on entropy production of nanofluid over permeable MHD stretching sheet at quadratic velocity and viscous dissipation, Case Stud. Therm. Eng. 45 (May 2023), 102992, https://doi.org/10.1016/J.CSITE.2023.102992.

[20] S. Alqaed, J. Mustafa, H.S. Aybar, B. Jamil, M.A. Alharthi, Investigation of thermal entropy generation and nanofluid flow in a new heatsink with the effect of nanoparticles shape, Case Stud. Therm. Eng. 36 (Aug. 2022), 102198, https://doi.org/10.1016/J.CSITE.2022.102198.

[21] Bhattad, J. Sarkar, P. Ghosh, Effects of nanoparticle shape and size on the thermohydraulic performance of plate evaporator using hybrid nanofluids, J. Therm. Anal. Calorimetry 143 (1) (Jan. 2021) 767–779, https://doi.org/10.1007/s10973-019-09146-z/figures/16.

[22] A. Bhattad, Exergy analysis of plate heat exchanger with graphene alumina hybrid nanofluid: experimentation, Int. J. Exergy 33 (3) (2020) 254–262, https://doi.org/10.1504/IJEX.2020.110863.

[23] K.B. Anoop, T. Sundararajan, S.K. Das, Effect of particle size on the convective heat transfer in nanofluid in the developing region, Int. J. Heat Mass Tran. 52 (9–10) (Apr. 2009) 2189–2195, https://doi.org/10.1016/j.ijheatmasstransfer.2007.11.063.

[24] A. Bhattad, J. Sarkar, P. Ghosh, 10.1142/S2010132518500037, Energy-Economic Analysis of Plate Evaporator Using Brine-Based Hybrid Nanofluids as Secondary Refrigerant, vol. 26, 2018, https://doi.org/10.1142/S2010132518500037, 1, Mar.

[25] S. Suseel Jai Krishnan, M. Momin, C. Nwaokocha, M. Sharifpur, J.P. Meyer, An empirical study on the persuasive particle size effects over the multi-physical properties of monophase MWCNT-Al2O3 hybridized nanofluids, J. Mol. Liq. 361 (2022), 119668, https://doi.org/10.1016/j.molliq.2022.119668.

[26] M. Shahul Hameed, S. Suresh, R.K. Singh, Comparative study of heat transfer and friction characteristics of water-based Alumina–copper and Alumina–CNT hybrid nanofluids in laminar flow through pipes, J. Therm. Anal. Calorimetry 136 (1) (2019) 243–253, https://doi.org/10.1007/s10973-018-7898-z. Apr.

[27] S. Osman, M. Sharifpur, J.P. Meyer, Experimental investigation of convection heat transfer in the transition flow regime of aluminum oxide-water nanofluids in a rectangular channel, Int. J. Heat Mass Tran. 133 (2019) 895–902, https://doi.org/10.1016/j.ijheatmasstransfer.2018.12.169.

[28] L.S. Sundar, M.K. Singh, A.C.M. Sousa, Enhanced heat transfer and friction factor of MWCNT-Fe3O4/water hybrid nanofluids, Int. Commun. Heat Mass Tran. 52 (Mar. 2014) 73–83, https://doi.org/10.1016/j.icheatmasstransfer.2014.01.012.

[29] C. Pak, Y.I. Cho, Hydrodynamic and heat transfer study of dispersed fluids with submicron metallic oxide particles, Exp. Heat Tran. 11 (2) (1998) 151–170, https://doi.org/10.1080/08916159808946559.

[30] L. Syam Sundar, M.T. Naik, K.V. Sharma, M.K. Singh, T.C. Siva Reddy, Experimental investigation of forced convection heat transfer and friction factor in a tube with Fe 3O 4 magnetic nanofluid, Exp. Therm. Fluid Sci. 37 (Feb. 2012) 65–71, https://doi.org/10.1016/j.expthermflusci.2011.10.004.

[31] M.T. Naik, L.S. Sundar, Heat transfer and friction factor with water/propylene glycol-based CuO nanofluid in circular tube with helical inserts under transition flow regime, Heat Tran. Eng. 35 (1) (Jan. 2014) 53–62, https://doi.org/10.1080/01457632.2013.810451.

[32] J.P. Meyer, T.J. McKrell, K. Grote, The influence of multi-walled carbon nanotubes on single-phase heat transfer and pressure drop characteristics in the transitional flow regime of smooth tubes, Int. J. Heat Mass Tran. 58 (1–2) (2013) 597–609, https://doi.org/10.1016/j.ijheatmasstransfer.2012.11.074.

[33] S.I. Abu-Eishah, Correlations for the thermal conductivity of metals as, Int. J. Thermophys. 22 (6) (2001) 1855–1868.

[34] O. Popiel, J. Wojtkowiak, Simple formulas for thermophysical properties of liquid water for heat transfer calculations (from 0°c to 150°c), Heat Tran. Eng. 19 (3) (1998) 87–101, https://doi.org/10.1080/01457639808939929.

[35] G. Huminic, A. Huminic, A numerical approach on hybrid nanofluid behaviour in laminar duct flow with various cross sections, J. Therm. Anal. Calorimetry 140 (5) (2020), https://doi.org/10.1007/s10973-019-08990-3.

[36] G. Huminic, A. Huminic, The heat transfer performances and entropy generation analysis of hybrid nanofluids in a flattened tube, Int. J. Heat Mass Tran. 119 (2018), https://doi.org/10.1016/j.ijheatmasstransfer.2017.11.155.

[37] V. Gnielinski, New equations for heat and mass transfer in turbulent pipe and channel flow, Int. J. Chem. Eng. 16 (2) (1976) 359–368. Accessed: Apr. 10, 2023. [Online]. Available: https://cir.nii.ac.jp/crid/1571980075607043456.bib?lang=en.

[38] R.H. Notter, C.A. Sleicher, A solution to the turbulent Graetz problem—III Fully developed and entry region heat transfer rates, Chem. Eng. Sci. 27 (11) (Jan. 1972) 2073–2093, https://doi.org/10.1016/0009-2509(72)87065-9.

[39] J.P. Meyer, J.A. Olivier, Transitional flow inside enhanced tubes for fully developed and developing flow with different types of inlet disturbances: Part I - adiabatic pressure drops, Int. J. Heat Mass Tran. 54 (7–8) (Mar. 2011) 1587–1597, https://doi.org/10.1016/j.ijheatmasstransfer.2010.11.027.

[40] H.R. Nagendra, Interaction of free and forced convection in horizontal tubes in the transition regime, J. Fluid Mech. 57 (2) (1973) 269–288, https://doi.org/10.1017/S0022112073001151.

[41] J. Ghajar, L.-M. Tam, Heat Transfer Measurements and Correlations in the Transition Region for a Circular Tube with Three Different Inlet Configurations, 1994.

[42] M. Everts, J.P. Meyer, Heat transfer of developing and fully developed flow in smooth horizontal tubes in the transitional flow regime, Int. J. Heat Mass Tran. 117 (Feb. 2018) 1331–1351, https://doi.org/10.1016/j.ijheatmasstransfer.2017.10.071.

[43] F. Andrade, A.S. Moita, A. Nikulin, A.L.N. Moreira, H. Santos, Experimental investigation on heat transfer and pressure drop of internal flow in corrugated tubes, Int. J. Heat Mass Tran. 140 (Sep. 2019) 940–955, https://doi.org/10.1016/j.ijheatmasstransfer.2019.06.025.
[44] M. Mehrali, et al., Heat transfer and entropy generation analysis of hybrid graphene/Fe3O4 ferro-nanofluid flow under the influence of a magnetic field, Powder Technol. 308 (2017), https://doi.org/10.1016/j.powtec.2016.12.024.
[45] A. J. G. Yunus A. Cengal, "Heat and Mass Transfer: Fundamentals and Applications," https://books.google.com/books/about/Heat_and_Mass_Transfer_Fundamentals_and.html?id=B89MnwEACAAJ..